Deep-Sea Research Part II xxx (xxxx) 105209

Contents lists available at ScienceDirect

Deep-Sea Research Part II

journal homepage: www.elsevier.com/locate/dsr2

Influence of sea surface wave-dependent roughness on summer precipitation over the Southeastern United States

Haixia Shan[a, b, c], Changming Dong[a, b, *], Jun-Hong Liang[c, d, e]

[a] School of Marine Sciences, Nanjing University of Information Science & Technology, Nanjing, 210044, China
[b] Southern Marine Science and Engineering Guangdong Laboratory (Zhuhai), Zhuhai, 519000, China
[c] Department of Oceanography and Coastal Sciences, Louisiana State University, Baton Rouge, LA, 70803, USA
[d] Center for Computation and Technology, Louisiana State University, Baton Rouge, LA, USA
[e] Coastal Studies Institute, Louisiana State University, Baton Rouge, LA, USA

ABSTRACT

To study the influence of ocean surface roughness on summer precipitation over the southeastern United States, we perform singular value decomposition (SVD) analysis between the mean summer precipitations and the significant wave height from 1979 to 2017 over the Gulf of Mexico (GOM). The first dominant mode shows that the swell energy in the northern GOM is much larger than that in the southern GOM, especially over the region adjacent to the southeastern United States (SE-US). Meanwhile, the precipitation in the SE-US is much heavier than the other regions. Composite analysis shows that when the first pattern takes place, the wind speed is much smaller near the region of the SE-US, the swell energy is much stronger. There is a cyclonic wind anomaly at 850 hPa over the SE-US, which results in much stronger upward motion, therefore much heavier rainfall in this region. To further study the effect of the swell on the precipitation in the SE-US, we also design two numerical experiments using the Coupled Ocean-Atmosphere-Wave-Sediment Transport (COAWST) Modelling System. In the control (CTL) experiment, the popular Charnock aerodynamical roughness length parameterization is adopted. In the other experiment, a newly developed wave-dependent roughness scheme is used. The precipitation in the SE-US is better simulated in the wave-dependent roughness experiment than in the CTL experiment. In summer, the 10-m wind speed is much weaker in the northeastern Gulf of Mexico, and that means the swell is dominant in this region. The wave-dependent surface roughness strengthens the wind, which means that the momentum flux is transferred from the ocean to the atmosphere under swell dominant conditions. The increase of the shear term and the cyclonic wind anomaly in the lower layers of the atmosphere leads to a stronger upward motion which makes rainfall much heavier in the SE-US.

1. Introduction

The wind stress at the sea surface represents the momentum exchange across the air-sea interface, which can influence many aspects of air-sea interactions, such as the generation of capillarity and gravity surface waves, ocean currents, and the mixed layers (Babanin et al., 2012; Grachev and Fairall, 2001). The momentum exchange is the main issue for many recent studies highlighting the impact of ocean waves on the dynamical processes across the air-sea interface (Smedman et al., 2003; Hanley and Belcher, 2008; Carlsson et al., 2009; Sullivan and McWilliams, 2010; Sullivan et al., 2014; Jenkins et al., 2012; Rutgersson and Sullivan, 2005; Wahle et al., 2017; Zou et al., 2017, 2018). Sea surface roughness is one of the important factors for understanding the relation between surface wind and air-sea momentum flux. The modification of momentum, enthalpy and moisture exchanges by the sea surface roughness affects the marine atmospheric boundary layer (MABL) processes. A good understanding of the momentum transfer between the wave field and the atmosphere is necessary. The classical Charnock relation (Charnock, 1955) is often adopted for atmospheric and oceanic modeling to calculate the air-sea momentum flux, which does not explicitly take into account the wave-state effects on the sea surface roughness.

wave effects are commonly thought to be confined within a thin layer above the water surface and are usually modeled as an aerodynamic roughness length in atmospheric circulation models. However, field observations, over Lake Ontario by Drennan et al. (1999), Baltic Sea by Smedman et al. (1994), the Atlantic and Pacific Oceans by Donelan et al. (1997) and Grachev and Fairall (2001)) and numerical modelling (Sullivan et al. 2000, 2008; Rutgersson and Sullivan 2005; Nilsson et al., 2012; Wu et al., 2017) have shown that the atmospheric surface layer can be strongly modulated by waves, especially swell wave.

The southern United States (US) is vulnerable to floods, droughts, hurricanes, and severe thunderstorms. Precipitation in this region is strongly affected by moisture transport from the Gulf of Mexico and is also related to the large-scale processes, including El Niño-Southern Oscillation (ENSO) (e.g., Arcodia et al., 2020), North Atlantic Oscillation (NAO) (e.g.,Schubert et al., 2009), North Atlantic subtropical high

---

[*] Corresponding author. School of Marine Sciences, Nanjing University of Information Science & Technology, Nanjing, 210044, China.
E-mail address: cmdong@nuist.edu.cn (C. Dong).

https://doi.org/10.1016/j.dsr2.2022.105209
Received 30 April 2022; Received in revised form 4 September 2022; Accepted 17 October 2022
0967-0645/© 20XX

(NASH) (e.g., Li et al., 2011), and the Great Plains low-level jet (GPLLJ) (e.g., Weaver and Nigam 2008). Ocean surface waves can play an active role in the climate systems. However, the effect of wave-dependent roughness on the climate systems is not well understood. Shimura et al. (2017) implemented wave-dependent surface roughness within the GCMs. They found that in the climate simulations with wave-dependent roughness, the reduced roughness and enhanced wind speeds in the tropics (enhanced trade winds) lead to an enhancement of the Hadley circulation. The spatial and temporal distribution of precipitation is also changed by the wave-dependent sea surface roughness.

The work presented here focuses on understanding how wave-dependent roughness impacts precipitation in the southeastern U.S. To achieve the objective, both data analysis using the singular value decomposition (SVD; Bretherton and SmithWallace, 1992; Wallace et al., 1992) and the numerical simulations using a coupled atmosphere-wave model are conducted. The atmosphere-wave interaction is modeled with two different parameterizations for sea surface roughness. One is a wind-dependent roughness parameterization (Porchetta et al., 2019) and the other is a wave-dependent roughness (Charnock, 1955). The impacts of wave-dependent roughness on the atmospheric are investigated by comparing the wave-dependent simulation with those that have only wind-dependent roughness. The rest of the paper is organized as follows, Section 2 presents data and methods, section 3 introduces the model and the configuration, Section 4 is the results, the discussions and conclusions are followed by Section 5.

2. Data and methods

The significant wave height, meridional and zonal 10 m wind, 850 hPa geopotential height and wind vectors are from ERA Interim product (Dee et al., 2011, 2014). ERA-Interim product can be downloaded from ECMWF's data archives, it has a horizontal spatial resolution of 0.75° × 0.75° and 60 vertical pressure layers from the surface to 0.1 hPa. Its coverage period begins in January 1979 to August 2019. The four daily analyses at 0000, 0600, 1200, and 1800 UTC are obtained by four-dimensional variational (4D-VAR) analysis systems with a 12 h analysis window (Courtier et al., 1994; Simmons et al., 1999). The wave-model component of ERA-Interim is based on the 3rd generation spectral wave model (WAM model) and has a horizontal resolution of 110 km. The wave model is run with shallow water physics where appropriate and discretized using 24 directions and 30 frequencies. More information can be found in Berrisford et al. (2011).

The gridded daily precipitation data used in this study is the National Oceanic and Atmospheric Administration (NOAA) Climate Prediction Center (CPC) Daily US Unified Gauge-Based Analysis of Precipitation Data (Chen et al., 2008), which is available from https://psl.noaa.gov/data/gridded/data.unified.daily.conus.html. The gauge analysis here covers the United States on a fine-resolution of 0.25° × 0.25°and is quantitatively consistent with that covering the global land on a coarser resolution (i.e., 0.5°). The CPC analysis provides 24-h precipitation accumulations each day (1200-1200 UTC), and it spans from 1948 to present.

Our primary tool for data analysis is SVD, a technique designed to identify pairs of spatial patterns describing the maximum temporal covariance between two fields, for example, precipitation and significant wave height. As input to the SVD routine, we use anomaly fields normalized by the standard deviation at each grid point. We perform SVD analysis between the mean summer precipitation fields (left field) and the significant wave height (right field) from 1979 to 2017 over the Gulf of Mexico (GOM). The summer season is referred to June-July-August (JJA). Composite analysis is also used in this study, which is a useful tool to smooth out the anomalies of individual cases and refine the most prominent dynamic and thermodynamic features.

3. Model description and configuration

The model used is the Coupled Ocean-Atmosphere-Wave-Sediment Transport (COAWST) Modelling System (Warner et al., 2010), which includes three state-of-the-art advanced numerical model components representing the atmosphere, ocean and wave environments. Previously, the COAWST model has been applied to study wave-current interaction in the Gulf of Mexico (Abolfazli et al., 2020). In this study, the modelling system is consisted of two model components: atmosphere (Weather Research and Forecasting, WRF) and wave (Simulating Waves Nearshore, SWAN). SWAN is coupled to WRF model through the Model Coupling Toolkit (Larson et al., 2005).

WRF is the next generation, fully compressible, non-hydrostatic, prognostic model suitable for idealized and realistic numerical simulations of the atmosphere, allowing to run on different scales ranging from synoptic to mesoscale. The model with the Advanced Research WRF (ARW) dynamical core (Skamarock et al., 2008) is used in this study, it uses a terrain-following hydrostatic-pressure coordinate in the vertical. Over the land, the model has four soil layers, and the unified Noah land-surface model (Chen and Dudhia, 2001) is used. The other physical options include the Rapid Radiative Transfer Model (RRTM) longwave radiation (Mlawer et al., 1997), Dudhia shortwave radiation (Dudhia, 1989); the Kain-Fritsch cumulus parameterization scheme (Kain, 2004), the WRF single moment 6-class (WSM 6) microphysics scheme (Hong and Lim, 2006), and the Mellor-Yamada-Nakanishi and Niino (MYNN) planetary boundary layer (PBL) scheme (Nakanishi and Niino, 2006).

The SWAN model is the third-generation, phase averaged, wind wave model based on the spectral action balance equation (Booij et al., 1999). In this study, the exponential growth of wind input and whitecapping parameterization developed by Komen et al. (1984) is used, and the parameterization for bottom friction is the one based on the empirical JONSWAP formulation (Hasselmann et al., 1973). The depth-induced wave breaking is included using the parameterization of Battjes and Janssen (1978) with proportionality coefficient of the rate of dissipation ($\alpha = 1.0$) and the ratio$\gamma$of maximum individual wave height over depth ($\gamma = 0.73$).

To further investigate the possible influence of the swell on the precipitation in the SE-US, we also design two experiments (Table 1) using the COAWST model. In the control (CTL) experiment, the Charnock aerodynamical roughness length parameterization is used, where α is the Charnock parameter and is assumed to be constant (Charnock, 1955). This parameterization is intended to effectively for fully developed wind waves over deep water. The other parameterization is proposed by Porchetta et al. (2019) (hereafter abbreviated as PS2019), which modifies the parameterization by Drennan et al. (2003) that has a poor performance in regions of swell. Drennan et al. (2005) suggested that a more elaborated roughness length parameterization including not only the swell magnitude but also the direction of the swell waves could improve the model. In the PS2019 experiment, the dependence on the alignment between wind and wave directions has taken into account. Using this new roughness length parameterization in numerical models might facilitate a better representation of the momentum transfer between the sea surface and the atmosphere. The impacts of wave-

Table 1
The design of the experiments.

Experiment	Formula	Reference
CTL	$z_0 = \alpha \frac{u_*^2}{g} + 0.11 \frac{\nu}{u_*}, \alpha = 0.0185$	Fairall et al. (2003)
PS2019	$z_0 = 30.09 \ \cos(0.437\theta) H_s \left(\frac{u_*}{c_p}\right)^{3.4 \ \cos(-0.274\theta)} + 0.11 \frac{\nu}{u_*}$	Porchetta et al. (2019)

Where Hs represents the significant wave height, Cp the wave phase speed at the peak frequency.

dependent roughness on the atmospheric are investigated by comparing the wave-dependent simulation with those that have only wind dependent roughness.

The WRF model domain (the outer box in Fig. 1) is centered at 25°N, 88°W with dimensions of 296 × 246 horizontal grid points and spacing of 9 km, and 45 vertical levels, which are unevenly distributed in the vertical from the surface to 50 hPa (top of the model). The simulation was driven with initial conditions from National Centers for Environmental Prediction (NCEP) Climate Forecast System Reanalysis (CFSR) Version 2, and lateral boundary conditions are updated every 6 h. The analyses are available on the surface, and on 37 pressure levels from 1000 to 1 hPa, available from http://dss.ucar.edu/datasets/ds094.0/. The SWAN domain (the inner box in Fig. 1) is on a rectangular grid with a horizontal grid spacing of 5 km. The spectral directional resolution is 10°.

When coupling with SWAN model, WRF provides the wind speeds for the SWAN and it gets significant wave heights (Hwave), peak periods (Pwave) and peak wavelengths (Lwave) from the SWAN model in order to estimate the wave-dependent sea surface roughness (z_0) at the ocean-atmosphere interface according to Porchetta et al. (2019) every 30 min.

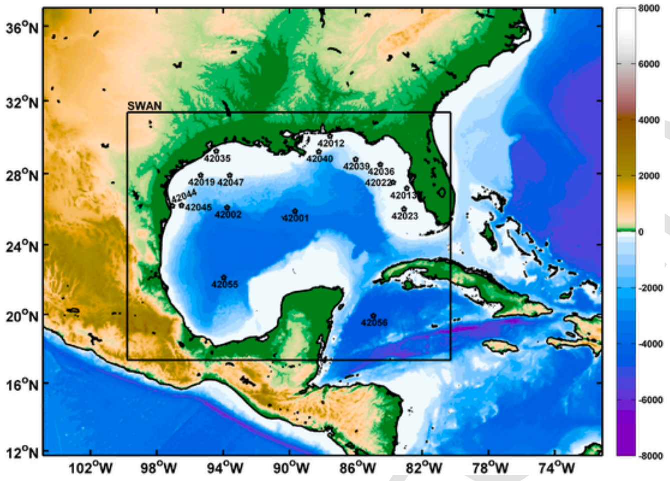

Fig. 1. The domain of the atmosphere-wave coupling model and topography (unit: m). The outer box is the WRF domain, and the inner box is for SWAN domain. The exact positions of 19 buoy stations are picked from the National Data Buoy Center (NDBC) are also marked with asterisk.

4. Results

Fig. 2 shows the first two significant coupled modes of co-variability with the first dominant mode explaining 48.6% while the second coupled mode explaining 34.6% of the total covariance. The significant wave height of Fig. 2c shows a similar pattern with the mean swell energy proportion to the total wave energy at the surface (Fig. 2a) following the method of Högström et al. (2015). In summer, the swell energy in the northern of GOM is much larger than that in the south part, especially over the region which is adjacent to the southeastern part of the United States (SE-US). When this wave pattern takes place, the precipitation (Fig. 2a) in the SE-US is much heavier than the other regions.When comes to the second mode, there will be more precipitation (Fig. 2b) in the northern part of the United States, and the maximum is located in the middle of the United State. At the meanwhile, there will be less precipitation in the SE-US. The significant wave height of Fig. 3d show a similar pattern with the mean magnitude of wind stress (Fig. 3b, calculated following the method of Zijlema et al. (2012)) in summer over the GOM. Overall, the mean magnitude of wind stress is much smaller in the eastern part of GOM than the western part.

Fig. 4 displays the normalized time coefficients series corresponding to the left and right singular vector in the first mode of SVD analysis of US precipitation and significant wave height in the summer from 1979 to 2017. These two time series have a correlation coefficient of about 0.7. Years with normalized time coefficients values larger than 0.5 standard deviation from the times series mean are defined as high (positive values) anomaly years. The low (negative values) anomaly years are referred to when the normalized time coefficients values smaller than −0.5 standard deviation. Fig. 5 shows the precipitation and significant wave height differences between the higher and lower anomaly years. Both of them depict a similar pattern with the first coupled mode displayed in Fig. 2. That is to say that when the precipitation in the SE-US is much heavier than the other regions, the significant wave height over the region which is adjacent to SE-US is much higher.

The analysis of satellite data and reanalysis wave hindcasts (Hanley et al., 2010; Semedo et al., 2011) shows that the swell is dominant at least 70% of the time in the mid and high latitudes and 95% dominant in the tropics. In summer, the wind is much weaker near the region of the SE-US, the swell energy is much stronger and is dominant in this region. It has been confirmed that there is upward momentum flux by

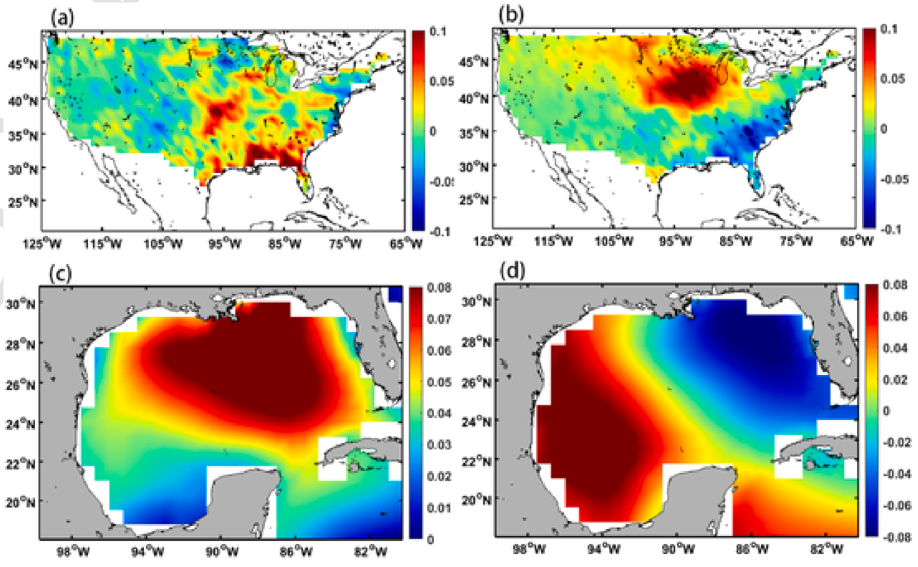

Fig. 2. The first (a,c) and second mode (b,d) of SVD analysis of US precipitation (top; unit:mm/h) and significant wave height (bottom; unit:m).

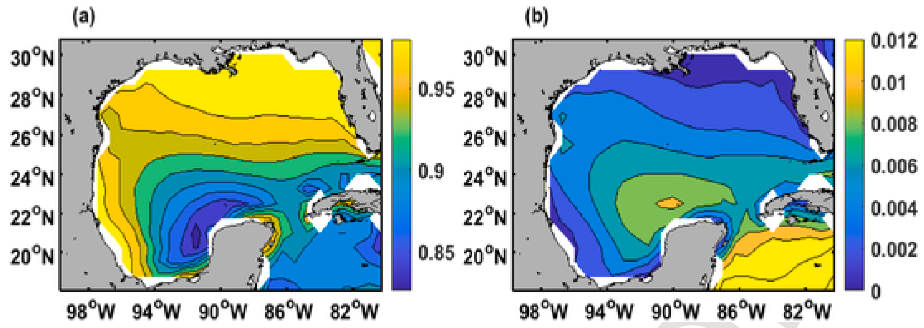

Fig. 3. The spatial distribution of the mean summer swell energy proportion to the total wave energy (a) at the surface and wind stress (b; unit:N/m^2) calculated from the ECMWF data.

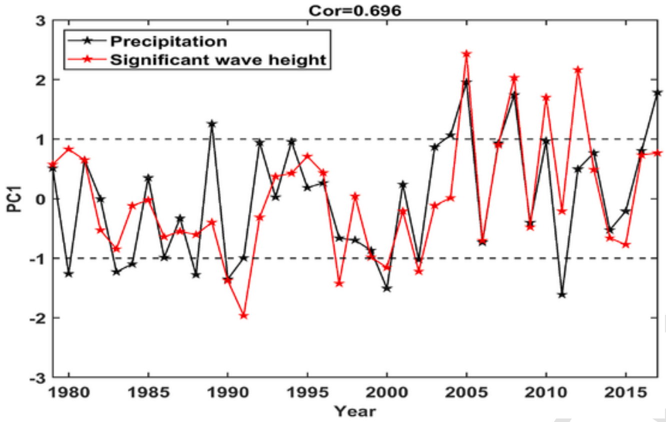

Fig. 4. The normalized time coefficients series corresponding to the left and right singular vector in the first mode of SVD analysis of mean summer US precipitation and significant wave height from 1979 to 2017.

several field measurements and numerical simulations (eg., Smedman et al., 1999; Grachev and Fairall, 2001; Sullivan et al., 2008; Semedo et al., 2009) under swell conditions, which means that the momentum flux is transferred from the wave field to the atmosphere. Fig. 6 displays the 850 hPa geopotential height and wind vector differences between the higher and lower anomaly years. It can be seen that there is a cyclonic wind anomaly at 850 hPa in the SE-US, which indicates that a stronger upward motion caused by the convergence in the lower of the atmosphere will make a heavier rainfall in this region.

To further investigate the possible influence of the swell on the precipitation in the SE-US, we also conduct two experiments (Table 1) using the COAWST model. Both the CTL and the PS2019 experiment is simulated from June to August in 2017. The year is chosen for the reason that both of normalized time coefficients values of the first mode are larger than 0.5 standard deviation from the times series mean.

To validate the model performance, we define two variables: Bias, and the root mean square error (RMSE). Bias is a way of measuring the mean error in the model and can show if the model tend to produce over- or underestimated values.

$$Bias = \frac{1}{N}\sum_{i=1}^{N} x_{mi} - x_{obsi} \qquad (1)$$

where N is number of grids, x_m is the modeled value and x_{obs} is the observed value. The root mean square error (RMSE) also describes the error in the model but gives more weight to outlying values thus providing further information about the spread in error size.

$$RMSE = \sqrt{\frac{1}{N}\sum_{i=1}^{N}\left(x_{mi} - x_{obsi}\right)^2} \qquad (2)$$

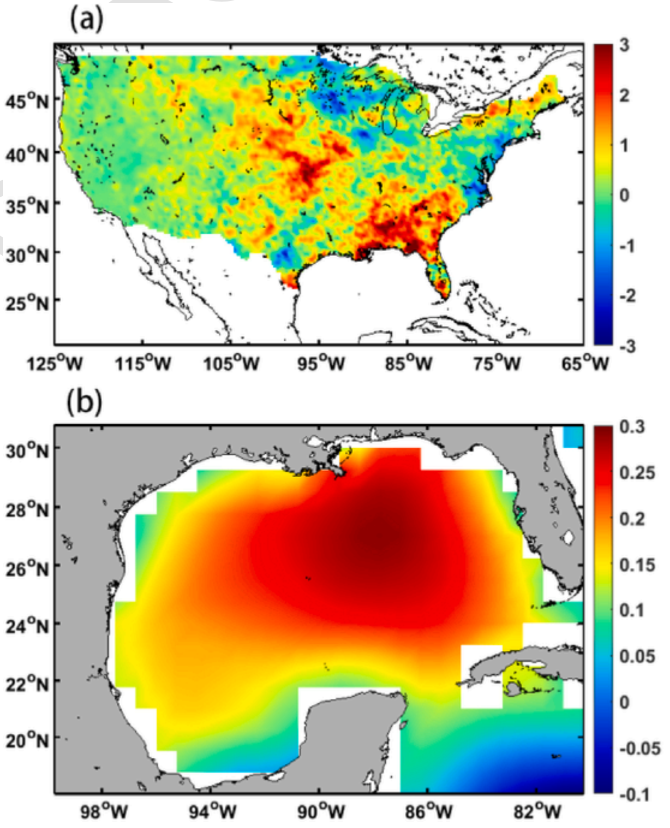

Fig. 5. The precipitation (a; unit: mm/h) and significant wave height (b; unit:m) differences between the higher years and lower years.

Nineteen buoy stations from the National Data Buoy Center (NDBC) are used for model validation of the 10-m wind speed. The locations of the selected buoys are also marked with asterisk in Fig. 1. Table 2 displays the monthly mean Bias and RMSE in this two experiments, it can be seen that in has a negative BIAS overall in the PS2019 experiment, while the RMSE is much smaller compared with the CTL experiments. Overall, the performance of the PS2019 experiment is much better.

Fig. 7 displays the spatial distribution of the mean precipitation in both experiments and the difference between them. In summer, the heavy precipitation is mainly located in the SE-US. The SE-US precipitation in the PS2019 experiment is evidently stronger that in the CTL experiment, which is the same as in the observation (Fig. 2a). Fig. 8 shows the spacial distribution of the 10-m wind speed. In the northeastern GOM, the 10-m wind speed is much smaller relative to the surrounding region. The swell can create significant variation in the drag at lower wind speeds and have moderate effect at higher wind speeds (Vincent et al., 2020). The wave-dependent surface roughness increases the simulated wind speed (Fig. 8c). The physical

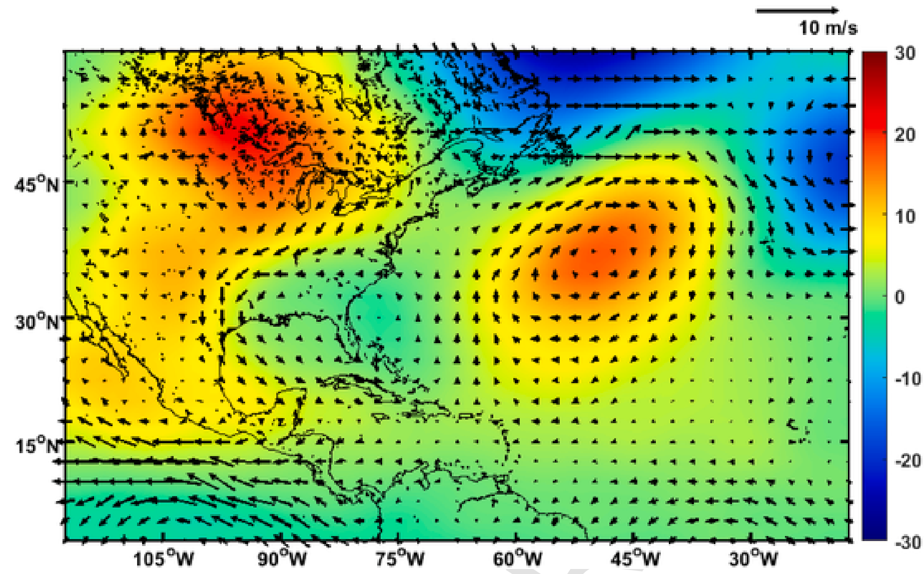

Fig. 6. The 850 hPa geopotential height (shading; unit: gpm) and wind vector differences (vectors; unit: m/s) between the higher and lower anomaly years.

Table 2
The mean BIAS and RMSE of the 10-m wind speed (unit:units: m/s) in different experiments compare with the buoy.

Station	BIAS		RMSE	
	CTL	PS2019	CTL	PS2019
42001	−0.27	−0.44	2.31	**2.3**
42002	−0.03	−0.42	2.46	**2.38**
42003	0.25	**0.12**	2.45	**2.37**
42012	0.27	**0.14**	2.68	**2.58**
42013	−0.03	−0.29	2.4	**2.35**
42019	−0.13	−0.61	2.65	**2.52**
42020	−0.43	−0.77	2.58	2.62
42022	0.03	−0.21	2.33	**2.3**
42023	−0.09	−0.21	2.18	**2.13**
42035	−0.14	−0.51	2.66	**2.54**
42036	0.54	**0.31**	2.63	**2.46**
42039	0.48	**0.31**	2.7	**2.58**
42040	0.44	**0.26**	2.87	**2.72**
42043	0.18	**−0.05**	2.74	**2.35**
42044	0.67	**0.36**	2.33	**2.21**
42045	0.32	**−0.04**	2.71	**2.62**
42047	−0.21	−0.55	2.8	**2.57**
42055	0.07	−0.25	2.6	**2.43**
42056	0.1	−0.28	2.35	**2.17**

explanation for this wind strengthening is that ocean waves supply momentum to the atmosphere instead of extracting momentum as they do in the wind wave conditions.

Fig. 9 shows the spatial distribution of 850 hPa wind and geopotential height difference, there is a cyclonic wind anomaly at 850 hPa in the SE-US, which is similar to that in Fig. 6. The vertically integrated moisture flux between 1000 hPa and 100 hPa (Fig. 10) in the PS 2019 experiment is much larger than that in the CTL experiment, which makes the precipitation much larger in the SE-US.

Turbulent kinetic energy (TKE) is a measure of turbulence and mixing in the atmosphere; it is directly related to the transport of momentum, heat and moisture through the MABL. Thus, understanding the variation of individual budget terms is crucial for understanding energy exchange mechanism within the MABL. The MYNN scheme in the WRF model is a popular, high-order closure PBL scheme. TKE prognostic equation in MYNN takes the form of

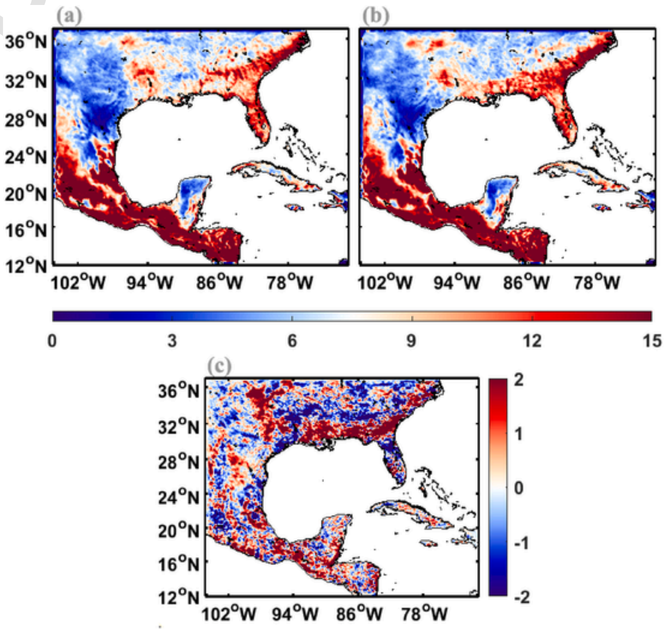

Fig. 7. The spacial distribution of the mean precipitation (shading; unit: mm/h) in CTL experiment (a) and PS2019 experiment (b), the difference between them is illustrated in (c).

$$\frac{\partial q^2}{\partial t} = 2\frac{g}{\bar{\theta}_0}\left\langle w'\theta' \right\rangle - 2\left(\left(\left\langle u'w' \right\rangle \frac{\partial \bar{u}}{\partial z} + \left\langle v'w' \right\rangle \frac{\partial \bar{v}}{\partial z}\right) - \frac{\partial \left\langle w'q^2 \right\rangle}{\partial z}\right) - 2\varepsilon \tag{3}$$

where q^2 ($= u'^2 + v'^2 + w'^2$) is twice the turbulent kinetic energy per unit mass, (u', v', w') are the turbulent velocity components, ($\bar{u}$, $\bar{v}$, $\bar{w}$) denote the mean components, and the angled brackets denote an ensemble average. Here θ' is the turbulent component of potential temperature and $\bar{\theta}$ is the mean component, and ε is the dissipation rate of TKE, given by

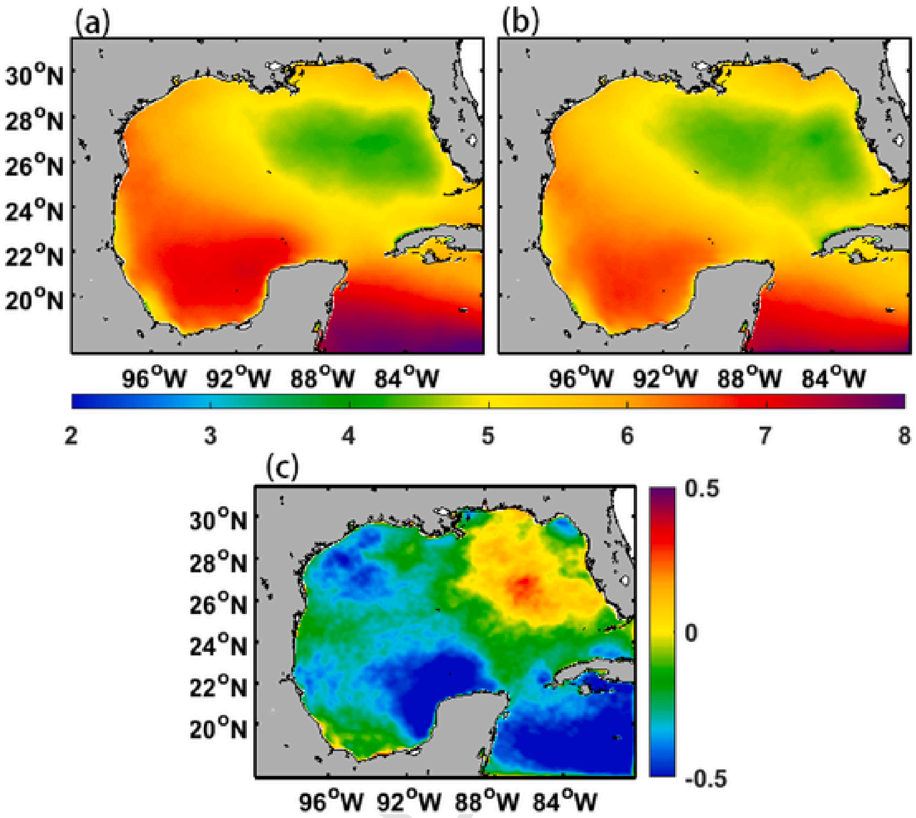

Fig. 8. The spacial distribution of the mean 10-m wind speed (shading; unit: m/s) in CTL experiment (a) and PS2019 experiment (b), the difference between them is illustrated in (c).

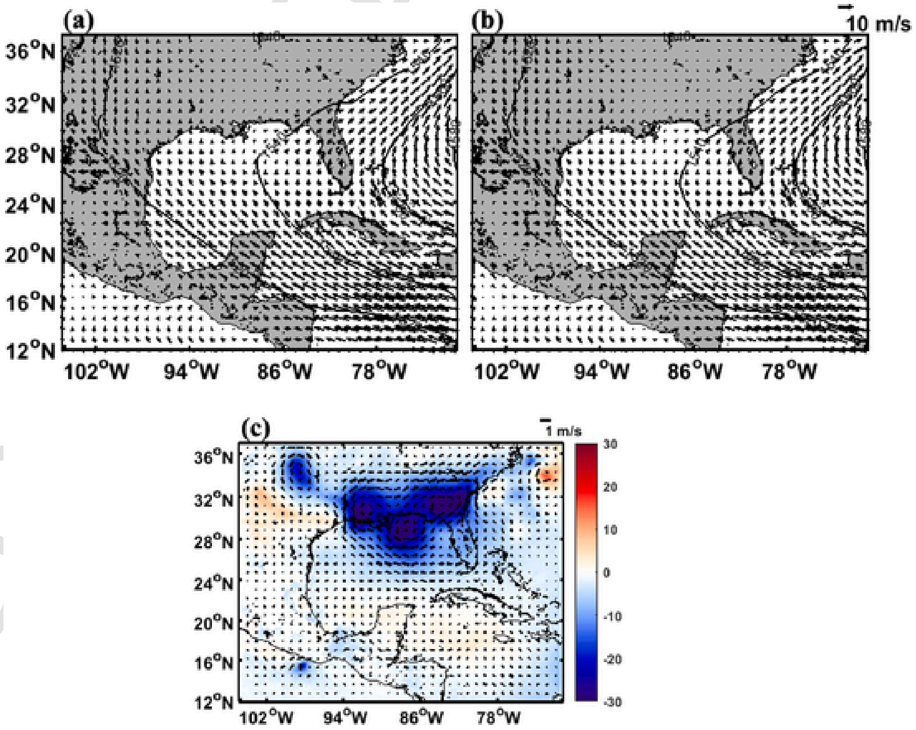

Fig. 9. The spacial distribution of the mean 850 hPa wind (vectors; unit: m/s) and the geopotential height (shading; unit: gpm) in CTL experiment (a) and PS2019 experiment (b), the difference between them is illustrated in (c).

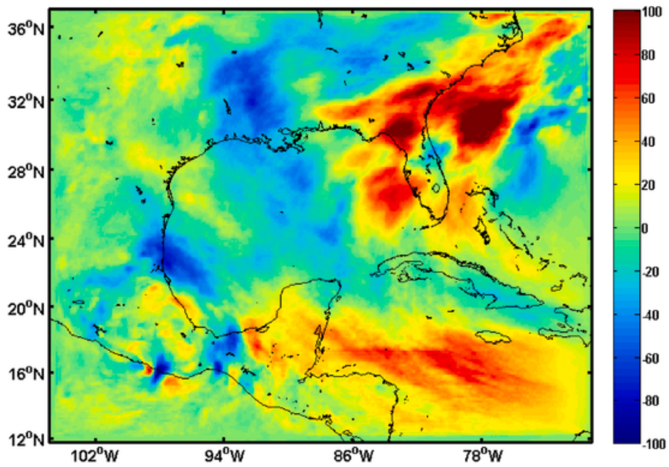

Fig. 10. The spacial distribution of the vertically integrated moisture flux between 1000 hPa and 100 hPa (unit: × 10^{-6} g/s/cm^2) difference between the two experiments.

$$\varepsilon = \frac{q^3}{B_1 L} \tag{4}$$

where B_1 is a closure constant and L is the mixing length.

The second-order turbulent fluxes such as $\langle u'w' \rangle$, are expressed in terms of gradient diffusion by

$$\begin{aligned} \langle u'w' \rangle &= -LqS_M \frac{\partial \bar{u}}{\partial z} \\ \langle v'w' \rangle &= -LqS_M \frac{\partial \bar{v}}{\partial z} \\ \langle w'\theta' \rangle &= -LqS_H \frac{\partial \bar{\theta}}{\partial z} \end{aligned} \tag{5}$$

where S_M and S_H are stability functions for momentum and heat, respectively.

The first term on the right-hand side (hereafter abbreviated as RHS) of equation (3) denotes buoyancy production (QBUOY). The other terms on the RHS denote shear production (QSHEAR), turbulence transport of TKE (QWT), and parameterized dissipation of TKE (QDISS), respectively; the formulations of these terms can be found in Nakanishi and Niino (2006). These terms can be output by the WRF model directly. Fig. 11 displays vertical distribution of the twice TKE, QBUOY, QSHEAR, and QWT difference averaged from 24°N to 35°N between the two experiments. The twice TKE has an increase in the region from 90°W to 82°W relative to the CTL experiment. The QSHEAR term shows a similar pattern with twice TKE, which has the largest difference compared to the other terms. The QBUOY and QSHEAR terms are sources for TKE, the QWT term can only redistribute the TKE vertically and the last one is a sink for TKE. The QSHEAR term is the main source for the change of TKE. In the summer, the wind speed is much smaller near the coastal region of the SE-US, the swell energy is much stronger and dominant in this region. There will be more momentum transferred from the wave field to the atmosphere, and shear term can contribute to the increase of TKE, making the MABL more turbulent. There is a cyclonic wind anomaly at 850 hPa in the SE-US, which indicates that a stronger upward motion caused by the convergence in the lower of the atmosphere leads to a heavier rainfall in this region.

5. Discussions and conclusions

We perform SVD analysis between the mean summer precipitations fields and the significant wave height from 1979 to 2017 over the Gulf of Mexico. In summer, the swell energy in the north of Gulf of Mexico is much larger than that in the south part, especially over the region which is adjacent to the SE-US region. When the swell energy dominates, the precipitation in the SE-US is much heavier than the other regions. Composite analysis of precipitation and significant wave height differences between the higher and lower anomaly years depict a similar pattern with the first coupled mode in the SVD analysis. In summer, the wind speed is much smaller near the region of the SE-US, the swell energy is much stronger. It has been found that there is upward momentum flux by several field campaigns and numerical simulations (eg., Smedman et al., 1999; Grachev and Fairall, 2001; Sullivan et al., 2008;

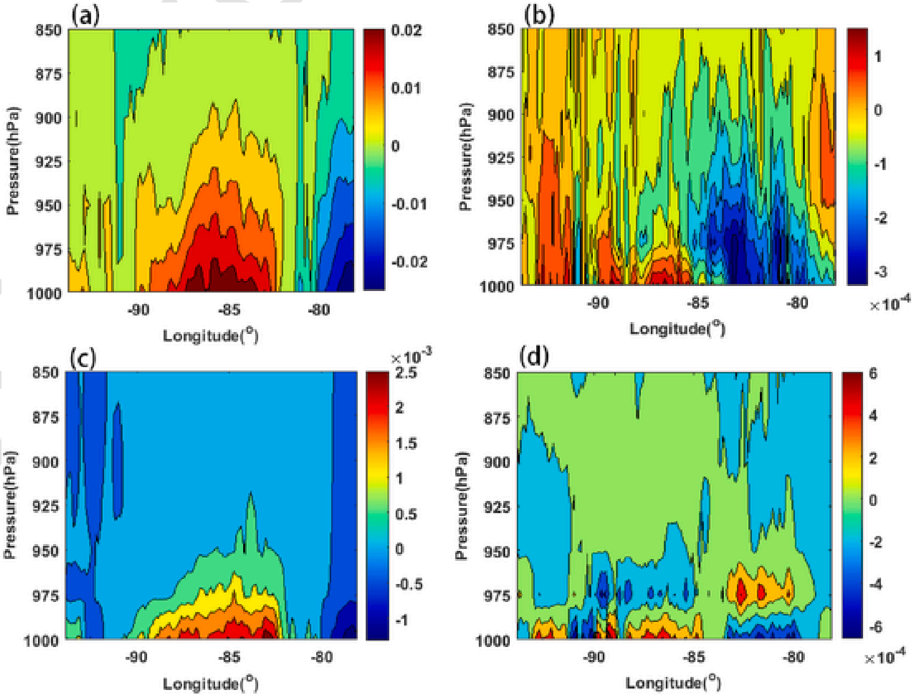

Fig. 11. The vertical distribution of the twice TKE (a; unit: m^2/s^2), QBUOY (b: unit: m^2/s^2), QSHEAR (c; unit: m^2/s^2), and QWT difference (d: unit: unit: m^2/s^2) averaged from 24°N to 35°N between the two experiments.

Semedo et al., 2009) under swell conditions, which means that more momentum flux is transferred from the wave field to the atmosphere.

To further study the effect of the swell on the precipitation over the SE-US, we also design two experiments using the COAWST model: One (CTL) using the Charnock aerodynamical roughness length parameterization (Charnock, 1955) and the other (PS2019) using a parameterization proposed by Porchetta et al. (2019), which takes into account the dependence on the alignment between wind and wave directions. Nineteen buoy stations from the National Data Buoy Center (NDBC) are used for model validation of the 10-m wind speed. Simulated with speed is much better in the PS2019 experiment than in the CTL experiment.

The simulated precipitation over the SE-US in the PS2019 experiment is evidently larger than that in the CTL experiment. In the northeastern Gulf of Mexico, the 10-m wind speed is much smaller relative to the surrounding region. The wave-dependent surface roughness will make the wind speed increase. There will be more momentum transferred from the wave field to the atmosphere, and shear term can contribute to the increase of TKE, making the MABL more turbulent. At the same time, there is a cyclonic wind anomaly at 850 hPa in the SE-US, which indicates that a stronger upward motion caused by the convergence in the lower of the atmosphere will make a heavier rainfall in this region. The vertically integrated moisture flux in the PS2019 experiment is much larger than that in the CTL experiment, which makes the precipitation much heavier in the SE-US.

Transfers of momentum and heat flux between the atmosphere and wave play an important role in weather and climate. Predicting the evolution of sea states under wind forcing in the ocean through atmosphere-wave coupled systems requires a fundamental understanding of the mechanisms of atmosphere-wave interaction. The wave-dependent physical processes are either parameterized simply using ocean surface winds or are not considered in many other atmospheric models. An inaccurate sea surface roughness parametrization is likely to contribute to systematic errors in the large-scale circulations within GCM simulations.

In addition, ocean waves are generally thought to act as a drag on the surface wind with a downward momentum transfer from the atmosphere into the waves. Observations (Smedman et al., 1994; Donelan et al., 1997; Drennan et al., 1999; Grachev and Fairall, 2001) during swell dominated conditions have reported that momentum can also be transferred from the waves into the atmosphere. This upward momentum transfer leads to an acceleration of the wind near the free surface, most of the atmosphere-ocean coupled models only allow the momentum transfer to be directed from the atmosphere to the ocean. Sea surface roughness parameterization that includes the angle between the wind and the wave direction is consistent with the wind profiles obtained by the large eddy simulation (LES) of Sullivan et al. (2000). Porchetta et al. (2019) showed that although the wave propagating direction deviates from the wind direction to a certain extent in the case of wind waves, the wave propagating direction deviates from the wind direction to a greater extent in the case of swell condition. This roughness parameterization can improve model performance in the swell dominated regions, which will be an effective method to study the influences of the swell to the precipitation in the SE-US. In this work, we do not consider ocean circulation in order to study impacts of wave-dependent roughness on atmospheric climate. Investigation of impacts on atmosphere-ocean climate is the next step of this work.

Author contributions

Haixia shan: Conceptualization, Methodology,Visualization, Writing Original draft preparation, Changming Dong: Conceptualization, Methodology, Resources, Funding acquisition, review and editing, Jun-Hong Liang: Conceptualization, Methodology, Resources, review and editing.

Declaration of competing interest

The authors declare that they have no known competing financial interests or personal relationships that could have appeared to influence the work reported in this paper.

All persons who have made substantial contributions to the work reported in the manuscript, including those who provided editing and writing assistance but who ate not authors, are named in the Acknowledgments section of the manuscript and have given their written permission to be named. If the manuscript does not include Acknowledgments, it is because the authors have not received substantial contributions from non-authors.

Data availability

Data will be made available on request.

Acknowledgments

H.S and C.D were supported by the National Key Research and Development Program of China (No. 2017YFA0604104), the National Natural Science Foundation of China (No.42192562), the Startup Foundation for Introducing Talent of NUIST (No. 2018r003), and the Priority Academic Program Development of Jiangsu Higher Education Institutions (PAPD). JHL was supported by the National Science Foundation through grant OCE-1945502.

References

Abolfazli, E., Liang, J.-H., Fan, Y., Chen, Q.J., Walker, N.D., Liu, J., 2020. Surface gravity waves and their role in ocean-atmosphere coupling in the Gulf of Mexico. J. Geophys. Oceans 125, e2018JC014820.

Arcodia, M.C., Kirtman, B.P., Siqueira, L.S.P., 2020. How MJO teleconnections and ENSO interference impacts U.S. precipitation. J.Climate. 33, 4621–4640.

Babanin, A., Onorato, M., Qiao, F., 2012. Surface waves and wave-coupled effects in lower atmosphere and upper ocean. J. Geophys. Res. 117, C00J01. https://doi.org/10.1029/2012JC007932.

Battjes, J.A., Janssen, J.P.F.M., 1978. Energy loss and set-up due to breaking of random waves. In: Proceedings of 16th International Conference on Coastal Engineering, ASCE. pp. 569–587.

Berrisford, P., Kållberg, P., Kobayashi, S., Dee, D., Uppala, S., Simmons, A.J., Poli, P., Sato, H., 2011. Atmospheric conservation properties in ERA-interim. Q. J. Roy. Meteorol. Soc. 137, 1381–1399.

Booij, N., Ris, R.C., Holthuijsen, L.H., 1999. A third-generation wave model for coastal regions: 1. Model description and validation. J. Geophys. Res. 104 (C4), 7649–7666. https://doi.org/10.1029/98JC02622.

Bretherton, C.S., Smith, C., Wallace, J.M., 1992. An intercomparison of methods for finding coupled patterns in climate data. J. Clim. 5, 541–560.

Carlsson, B., Rutgersson, A., Smedman, A.-S., 2009. Impact of swell on simulations using a regional atmospheric climate model. Tellus 61, 527–538.

Charnock, H., 1955. Wind stress on a water surface. Q. J. Roy. Meteorol. Soc. 81, 639–640.

Chen, F., Dudhia, J., 2001. Coupling an advanced land surface-hydrology model with the penn state-NCAR MM5 modeling system. Part I: model implementation and sensitivity. Mon. Weather Rev. 129, 569–585.

Chen, M., Shi, W., Xie, P., Silva, V., Kousky, V.E., Wayne Higgins, R., Janowiak, J.E., 2008. Assessing objective techniques for gauge-based analyses of global daily precipitation. J. Geophys. Res. 113, D04110. https://doi.org/10.1029/2007JD009132.

Courtier, P., Thépaut, J.-N., Hollingsworth, A., 1994. A strategy for operational implementation of 4D-Var, using an incremental approach. Quart. J. Roy. Meteor. Soc. 120, 1367–1387. https://doi.org/10.1002/qj.49712051912.

Dee, D.P., Uppala, S.M., Simmons, A.J., Berrisford, P., Poli, P., Kobayashi, S., Andrae, U., Balmaseda, M.A., Balsamo, G., Bauer, P., Bechtold, P., Beljaars, A.C.M., van de Berg, L., Bidlot, J., Bormann, N., Delsol, C., Dragani, R., Fuentes, M., Geer, A.J., Haimberger, L., Healy, S.B., Hersbach, H., Hólm, E.V., Isaksen, L., Kållberg, P., Köhler, M., Matricardi, M., McNally, A.P., Monge-Sanz, B.M., Morcrette, J.-J., Park, B.-K., Peubey, C., de Rosnay, P., Tavolato, C., Thépaut, J.-N., Vitart, F., 2011. The ERA-Interim reanalysis: configuration and performance of the data assimilation system. Q. J. Roy. Meteorol. Soc. 137, 553–597.

Dee, D.P., Balmaseda, M., Balsamo, G., Engelen, R., Simmons, A.J., Thépaut, J.-N., 2014. Toward a consistent reanalysis of the climate system. Bull. Am. Meteorol. Soc. 95 (8), 1235–1248.

Donelan, M., Drennan, W., Katsaros, K., 1997. The air-sea momentum flux in conditions of wind sea and swell. J. Phys. Oceanogr. 27, 2087–2099.

Drennan, W., Graber, H., Donelan, M., 1999. Evidence for the effects of swell and unsteady winds on marine wind stress. J. Phys. Oceanogr. 29, 1853–1864.

Drennan, W., Graber, H.C., Hauser, D., Quentin, C., 2003. On the wave age dependence of wind stress over pure wind seas. J. Geophys. Res. 108, 8062.

Drennan, W., Taylor, P., Yelland, M., 2005. Parameterizing the sea surface roughness. J. Phys. Oceanogr. 35, 835–848.

Dudhia, J., 1989. Numerical study of convection observed during the winter monsoon experiment using a mesoscale two-dimensional model. J. Atmos. Sci. 46, 3077–3107.

Grachev, A., Fairall, C., 2001. Upward momentum transfer in the marine boundary layer. J. Phys. Oceanogr. 31, 1698–1710.

Hanley, K., Belcher, S., 2008. Wave-driven wind jets in the marine atmospheric boundary layer. J. Atmos. Sci. 65, 2646–2660.

Hanley, K., Belcher, S., Sullivan, P., 2010. A global climatology of wind–wave interaction. J. Phys. Oceanogr. 40, 1263–1282. https://doi.org/10.1175/2010JPO4377.1.

Hasselmann, K., Barnett, T.P., Bouws, E., Carlson, H., Cartwright, D.E., Enke, K., Ewing, J.A., Gienapp, H., Hasselmann, D.E., Kruseman, P., Meerburg, A., Mueller, P., Olbers, D.J., Richter, K., Sell, W., Walden, H., 1973. Measurements of wind-wave growth and swell decay during the joint north sea wave project (JONSWAP). Ergänzung zur Deut. Hydrogr. Z., Reihe A 12 (8), 95.

Högström, U., Sahlée, E., Smedman, A.S., Rutgersson, A., Nilsson, E., Kahma, K.K., Drennan, W.M., 2015. Surface stress over the ocean in swell-dominated conditions during moderate winds. J. Atmos. Sci. 72 (12), 4777–4795.

Hong, S.-Y., Lim, J.-O.J., 2006. The WRF single-moment 6-class microphysics scheme (WSM6). J. Korean Meteor. Soc. 42, 129–151.

Jenkins, A., Paskyabi, M., Fer, I., Gupta, A., Adakudlu, M., 2012. Modelling the effect of ocean waves on the atmospheric and ocean boundary layers. Energy Proc. 24, 166–175.

Kain, J.S., 2004. The Kain–Fritsch convective parameterization: an update. J. Appl. Meteorol. 43, 170–181.

Komen, G.J., Hasselmann, S., Hasselmann, K., 1984. On the existence of a fully developed windsea spectrum. J. Phys. Oceanogr. 14, 1271–1285.

Larson, J., Jacob, R., Ong, E., 2005. The model coupling toolkit: a new fortran90 toolkit for building multiphysics parallel coupled models. Int. J. High Perform. Comput. Appl. 19, 277–292. https://doi.org/10.1177/1094342005056115.

Li, W., Li, L., Fu, R., Deng, Y., Wang, H., 2011. Changes to the North Atlantic subtropical high and its role in the intensification of summer rainfall variability in the southeastern United States. J. Clim. 24, 1499–1506.

Mlawer, E.J., Taubman, S.J., Brown, P.D., Iacono, M.J., Clough, J.S.A., 1997. Radiative transfer for inhomogeneous atmospheres: RRTM, a validated correlated-k model for the longwave. J. Geophys. Res. 102 (D14), 16663–16682.

Nakanishi, M., Niino, H., 2006. An improved Mellor-Yamada level 3 model: its numerical stability and application to a regional prediction of advecting fog. Bound. Layer Meteor. 119, 397–407.

Nilsson, E., Rutgersson, A., Smedman, A.-S., Sullivan, P., 2012. Convective boundary-layer structure in the presence of wind-following swell. Q. J. Roy. Meteorol. Soc. 138, 1476–1489.

Porchetta, S., Temel, O., Muñoz-Esparza, D., Reuder, J., Monbaliu, J., van Beeck, J., van Lipzig, N., 2019. A new roughness length parameterization accounting for wind–wave (mis)alignment. Atmos. Chem. Phys. 19, 6681–6700. https://doi.org/10.5194/acp-19-6681-2019.

Rutgersson, A., Sullivan, P., 2005. The effect of idealized water waves on the turbulence structure and kinetic energy budgets in the overlying airflow. Dynam. Atmos. Oceans 38, 147–171.

Schubert, S., Gutzler, D., Wang, H., Dai, A., Delworth, T., Deser, C., Findell, K., Fu, R., Higgins, W., Hoerling, M., Kirtman, B., 2009. A U.S. CLIVAR project to assess and compare the responses of global climate models to drought-related SST forcing patterns: overview and results. J. Clim. 22, 5251–5272.

Semedo, A., Saetra, Ø., Rutgersson, A., Kahma, K., Pettersson, H., 2009. Wave-induced wind in the marine boundary layer. J. Atmos. Sci. 66 (8), 2256–2271.

Semedo, A., Suselj, K., Rutgersson, A., Sterl, A., 2011. A global view on the windsea and swell climate and variability from ERA-40. J. Clim. 24, 1461–1479.

Shimura, T., Mori, N., Takemi, T., Mizuta, R., 2017. Long-term impacts of ocean wave-dependent roughness on global climate systems. J. Geophys. Res. 122, 1995–2011. https://doi.org/10.1002/2016JC012621.

Simmons, A.J., Untch, A., Jakob, C., Kållberg, P., Unden, P., 1999. Stratospheric water vapour and tropical tropopause temperatures in ECMWF analyses and multi-year simulations. Quart. J. Roy. Meteor. Soc. 125, 353–386. https://doi.org/10.1002/qj.49712555318.

Skamarock, W.C., Klemp, J.B., Dudhia, J., Gill, D.O., Barker, M., Duda, M.G., Huang, X.-Y., Wang, W., Powers, J.G., 2008. A Description of the Advanced Research WRF Version 3.NCAR/TN-475+STR. NCAR TECHNICAL NOTE, p. 113.

Smedman, A.-S., Tjernström, M., Högström, U., 1994. The near-neutral marine atmospheric boundary layer with No surface shearing stress: a case study. J. Atmos. Sci. 51, 3399–3411.

Smedman, A.-S., Högström, U., Bergström, H., Rutgersson, A., Kahma, K., Pettersson, H., 1999. A case study of air-sea interaction during swell conditions. J. Geophys. Res. 104, 25833–25851.

Smedman, A.-S., Larsén, X.G., Högström, U., Kahma, K., Pettersson, H., 2003. Effect of sea state on the momentum exchange over the sea during neutral conditions. J. Geophys. Res. 108 (C11), 3367. https://doi.org/10.1029/2002JC001526.

Sullivan, P., McWilliams, J., 2010. Dynamics of winds and currents coupled to surface waves. Annu. Rev. Fluid Mech. 42, 19–42.

Sullivan, P., McWilliams, J., Moeng, C., 2000. Simulation of turbulent flow over idealized water waves. J. Fluid Mech. 80, 535–559.

Sullivan, P., Edson, J., Hristov, T., McWilliams, J., 2008. Large-eddy simulations and observations of atmospheric marine boundary layers above nonequilibrium surface waves. J. Atmos. Sci. 65, 1225–1245.

Sullivan, P., McWilliams, J., Patton, E., 2014. Large-eddy simulation of marine atmospheric boundary layers above a spectrum of moving waves. J. Atmos. Sci. 71, 4001–4027.

Vincent, C.L., Graber, H.C., Collins, III, C.O., 2020. Effect of swell on wind stress for light to moderate winds. J. Atmos. Sci. 77, 3759–3768.

Wahle, K., Staneva, J., Koch, W., Fenoglio-Marc, L., Ho-Hagemann, H., Stanev, E.V., 2017. An atmosphere–wave regional coupled model: improving predictions of wave heights and surface winds in the southern North Sea. Ocean Sci. 13 (2), 289–301.

Wallace, J.M., Smith, C., Bretherton, C.S., 1992. Singular value decomposition of wintertime sea surface temperature and 500-mbheight anomalies. J. Clim. 5, 561–576.

Warner, J.C., Armstrong, B., He, R., Zambonm, J.B., 2010. Development of a coupled ocean-atmosphere-wave-sediment transport (COAWST) modeling system. Ocean Model. 35, 230–244. https://doi.org/10.1016/j.ocemod.2010.07.010.

Weaver, S.J., Nigam, S., 2008. Variability of the great plains low-level jet: large-scale circulation context and hydroclimate impacts. J. Clim. 21, 1532–1551.

Wu, L., Rutgersson, A., Nilsson, E., 2017. Atmospheric boundary layer turbulence closure scheme for wind-following swell conditions. J. Atmos. Sci. 74 (7), 2363–2382. https://doi.org/10.1175/JAS-D-16-0308.1.

Zijlema, M., van Vledder, G. Ph, Holthuijsen, L.H., 2012. Bottom friction and wind drag for spectral wave models. Coast. Eng. 65, 19–26.

Zou, Z., Zhao, D., Liu, B., Zhang, J., Huang, J., 2017. Observation-based parameterizaion of air-sea fluxes in terms of wind speed and atmospheric stability under low-to-moderate wind conditions. J. Geophys. Res. 122 (5), 4123–4142.

Zou, Z., Zhao, D., Zhang, J., Li, S., Cheng, Y., Lv, H., Ma, X., 2018. The influence of swell on the atmospheric boundary layer under nonneutral conditions. J. Phys. Oceanogr. 48 (4), 925–936.